Numerical simulation by finite element modelling of diffusion and transient hydrogen trapping processes in plasma facing components

S. Benannoune, Y. Charles, J. Mougenot, M. Gaspérini, G. de Temmerman

Nuclear Materials and Energy 19 (2019) 42–46

Contents lists available at ScienceDirect

Nuclear Materials and Energy

journal homepage: www.elsevier.com/locate/nme

Numerical simulation by finite element modelling of diffusion and transient hydrogen trapping processes in plasma facing components

S. Benannoune[a], Y. Charles[a], J. Mougenot[a,*], M. Gaspérini[a], G. De Temmerman[b]

[a] Université Paris 13, Sorbonne Paris Cité, LSPM, CNRS UPR 3407, 99 avenue Jean-Baptiste Clément, Villetaneuse 93430, France
[b] ITER Organization, Route de Vinon-sur-Verdon, CS 90046, 13067, St. Paul Lez Durance Cedex, France

ARTICLE INFO

Keywords:
Hydrogen
Kinetic trapping
Modelling
Finite elements
Abaqus
User subroutine
Macroscopic Rate Equations

ABSTRACT

In order to simulate hydrogen charging and discharging cycles of mechanically loaded structures full 3D Macroscopic Rate Equation (MRE) modelling is proposed based on a finite element method (FEM). The model, implemented in the 3DS Abaqus software, uses a generalized transport equation, which accounts for mechanical fields, hydrogen transport and trapping, and their evolution with time. The influence of a-priori known thermal field has also been included. To ensure the solution convergence and the numerical stability, the trapping kinetic is introduced by using an approximation of the analytical solution the McNabb and Foster equation. Comparisons with a relevant 1D MRE code and with thermal programmed desorption (TPD) experimental results are performed on a 1D configuration to validate the model. Next, the model is used to simulate the tritium diffusion and trapping in a 2D geometry of interest in the upper plug of ITER tokamak, and results of tritium inventory are compared with an equivalent 1D calculation.

1. Introduction

Understanding and controlling hydrogen isotope (HI) inventory is a key factor for future fusion devices both to limit in-vessel retention and to increase the tritium-breeding ratio. HI transport and trapping can also lead to embrittlement of plasma-facing materials. Simulations of diffusion and trapping of HI in metals is commonly made using a full diffusion-trapping process kinetic description. Specific Macroscopic Rate Equations (MRE) codes [1–4], developed for plasma surface interactions, and based on the McNabb and Foster equation [5], allow description of transient trapping kinetics. Most of these MRE codes are dedicated to 1D problems, in which the influence of 3D defects (like gas bubbles) could be estimated [6]. However, a special focus has to be made to develop numerical models in order to estimate with more precision HI retention on 2D and 3D complex geometries.

This work is dedicated to the MRE extension to 3D configurations using finite element modelling (FEM), permitting solution of various initial boundary value problems. This constitutes an extension of previous work dedicated to perform generalized transport simulations accounting for stress-assisted diffusion [7–9], with a transient trapping process [10]. In order to ensure a compromise between reliable numerical convergence and reasonable computation cost of the implementations in FE codes, a new formulation based on a generalization Oriani's formulation [11] is developed to take accounts for transient HI trapping and its coupling with diffusion equation [12,13].

The first section summarizes the different approaches used to account for the HI trapping. The Generalized Oriani's Approximation (GOA) for the transient HI trapping and its validation are detailed. A specific section shows the capacity of the GOA to reproduce an experimental thermal programmed desorption (TPD). Last, the method is applied to the simulation of tritium retention over upper plug of ITER tokamak with a comparison with MRE 1D and 2D simulations is conducted in order to show the importance of 2D simulations relative to 1D approximation.

2. Generalized Oriani's Approximation

While dealing with hydrogen transport and trapping in materials, the hydrogen concentration C is generally decomposed into a trapped part C_T (atoms /m^3), and a diffusive one C_L (atoms/m^3). Based on mass conservation, the global equation of transport/trapping assisted by the hydrostatic pressure P_H leads to [7,14]:

$$\frac{\partial C_L}{\partial t} + \theta_T \frac{\partial N_T}{\partial t} + N_T \frac{\partial \theta_T}{\partial t} + \nabla . \left(-D_L \nabla C_L - D_L C_L \frac{V_H}{RT} \nabla P_H \right) = 0 \quad (1)$$

where N_T is the trap site density (vacancies, dislocations, grain boundaries…) in traps/m^3, N_L the interstitial site one in sites/m^3, whiles θ_T and θ_L are their occupancy which correspond respectively to

* Corresponding author.
E-mail address: jonathan.mougenot@lspm.cnrs.fr (J. Mougenot).

https://doi.org/10.1016/j.nme.2019.01.023
Received 30 July 2018; Received in revised form 25 January 2019; Accepted 25 January 2019
Available online 14 February 2019

the ratio C_T/N_T (atoms/trap) and C_L/N_L (atoms/site). D_L represents the bulk hydrogen diffusion coefficient, V_H the partial hydrogen molar volume, R the ideal-gas constant and T the temperature.

To model the transient trapping process, McNabb and Foster [5] proposed to solve the trap occupancy evolution:

$$\frac{\partial \theta_T}{\partial t} = p\theta_L(1-\theta_T) - k\theta_T \tag{2}$$

where p and k are material-dependent parameters related to trapping and detrapping respectively

According to Oriani [11], when trapping process is assumed to be instantaneous, a direct relationship is established between θ_L and θ_T:

$$K_T\theta_L = \frac{\theta_T}{1-\theta_T} \tag{3}$$

where $K_T = p/k$, p and k being material-dependent parameters.

To simulate the transient trapping, a numerical scheme able to solve simultaneously Eqs. (1) and (2) is needed, as in MRE codes based on finite difference scheme [2,6,15]. This coupling may induce crippling numerical costs in case of complex 3D problems.

An alternative way is here proposed, consisting in approximation of the solution of Eq (2) by an analytical formulation [12] which permits to obtain a direct relationship between θ_L and θ_T when accounting for the transient trapping:

$$\theta_T = \left(\theta_T^0 - \frac{p\theta_L}{p\theta_L + k}\right)\left[e^{-(p\theta_L+k)t}\right] + \frac{p\theta_L}{p\theta_L + k} \tag{4}$$

θ_T^0 is the value of θ_T at $t = 0$ (begin of each time step). The McNabb and Foster differential equation have been solved, also based on a θ_L time-independent assumption [12,13]. Eq. (4) appears then as an extension of the Oriani's approach for non-steady states evolution of θ_T; is worth noting that this approximation is simply an analytic solution of the McNabb and Foster equation for a fixed θ_L. This formulation, hereafter called “Generalized Oriani's Approximation” (GOA) ensures a correct convergence for large numerical schemes and can be implemented more easily than McNabb and Foster formulation in commercial numerical codes. The model has been implemented in 3DS Abaqus Finite Element (FE) software [16], using User Subroutines written in Fortran. The resolution of Eq. (1) is based on two User Subroutines: a UMAT one, dedicated the mechanical field computations (including the pressure gradient), and a UMATHT one, related to specific diffusion process. Computations are made using the ‘coupled temp-displacement’ scheme of Abaqus, or which both diffusion and mechanical problems are simultaneously solved [8,9]. Trapping is added in the UMATHT subroutine, considering C_T as an internal variable. To get a converged solution in Abaqus, it is mandatory to define in the UMATHT subroutine, on the one hand, the increment of flux and internal variables, knowing the C_L one, and on the other hand, $\partial C_T/\partial C_L$, linked to the Newton-Raphson scheme used in Abaqus. All of these values might be easily computed at each increment of the finite element computation using equations (3) or (4) (see [12] for details).

A validation of the GOA has been made by performing a simulation of H diffusion and trapping in a metallic sample with the geometry of a beam exposed to a 100 eV hydrogen plasma (with a flux of 2.5×10^{19} H.m^{-2}.s^{-1}), for three different bcc materials (tungsten, α-iron and low carbon steel). The computed trapped H concentrations are plotted along the beam axis for each material (the position $z = 0$ corresponding to the surface exposed to the plasma) and for each formulation: results for Oriani's and GOA's ones are obtained with Abaqus code whereas the results for McNabb and Foster's formulation are obtained with the MRE code HIIPC [3,6].

Fig. 1 summarizes the main results of this validation case. Details and material parameters are presented in [12]. The amount of H trapped increases with the exposure time and for each time the results for transient trapping are lower than results based on an instantaneous trapping assumption. For the low-C steel, the 3D equilibrium results are very different from the transient ones while the differences are much smaller for the other two materials; such a difference is due to the chosen exposure times [12], and the greater this time, the lower the difference between kinetic and transient trapping results. Results given by GOA and McNabb and Foster's formulations are similar for every configuration, allowing us to conclude that the GOA allows to get an accurate evaluation of the transient transport and trapping process.

3. Plasma exposure of tungsten and TPD spectrum reproduction

The GOA is extended to reproduce a thermal programmed desorption (TPD) spectrum measured experimentally by Ogorodnikova et al. [17]. Numerical simulations include three steps: first, during plasma exposure (duration 360 s), a deuterium plasma source (with a flux of 2.5×10^{19} D.m^{-2}.s^{-1}) is imposed at the surface, while transport and trapping occur in the sample; then the plasma source is switched off, and the sample is set HI loading free for 50 s, leading to a slow detrapping process. Last, a temperature ramp 8 K.s^{-1} is imposed, to speed up the HI detrapping, which corresponds to the TPD experiment. To obtain a good match of the experimental TPD spectrum, Hodille et al. [2] have proposed to account for three traps (two intrinsic traps and one induced by plasma exposure). Eq. (1) is consequently modified (without mechanical field influence on transport)

$$\frac{\partial C_L}{\partial t} + N_{T1}\frac{\partial \theta_{T1}}{\partial t} + N_{T2}\frac{\partial \theta_{T2}}{\partial t} + N_{T3}\frac{\partial \theta_{T3}}{\partial t} + \theta_{T3}\frac{\partial N_{T3}}{\partial t} - \nabla(D_L\nabla C_L) - \Gamma = 0 \tag{5}$$

where N_{Ti} and θ_{Ti} are respectively the i^{th} the trap site density and their related occupancies. N_{T1} and N_{T2} are constant during the simulation (respectively 1.0×10^{-3} at.fr and 4.0×10^{-4} at.fr), whereas the spatio-temporal evolution of N_{T3} is so that [17]:

$$N_{T3} = N_L W_m\left(1 - \exp\left[-\frac{(1-r)\Gamma\eta t}{N_L W_m}\right]\right) \tag{6}$$

where W_m (0.1 at.fr) is the maximum trap density; η (10^{-3}) the trap creation probability and Γ is the deterium source corresponding to the plasma exposition.

The GOA has thus been modified to allow the inclusion of multi-trapping and the influence of a known variation of a temperature field, considering that

$$\theta_{Ti} = \left(\theta_{Ti}^0 - \frac{p_i\theta_L}{p_i\theta_L + k_i}\right)\left[e^{-(p_i\theta_L+k_i)t}\right] + \frac{p_i\theta_L}{p_i\theta_L + k_i} \tag{7}$$

and

$$\frac{\partial \theta_{Ti}}{\partial t} = \left.\frac{\partial \theta_{Ti}}{\partial \theta_L}\right|_{t,T}\dot{\theta}_L + \left.\frac{\partial \theta_{Ti}}{\partial t}\right|_{\theta_L,T} + \left.\frac{\partial \theta_{Ti}}{\partial T}\right|_{t,\theta_L}\dot{T} \tag{8}$$

Convergence tests were done for large temperature time evolution (from 0.01 K/s up to 50 K/s) for the studied materials, in order to ensure the validity of the GOA for such applications. Due to the incremental implementation of the GOA in the software, convergence might be reach for small enough step times. Deuterium desorption flux versus temperature are presented on Fig. 2. Results obtained by the MRE HIIPC code with McNabb and Foster's formulation (thanks to trap parameters from [2]) reproduce correctly experimental values [17] and Abaqus results based on the GOA are similar to the MRE HIIPC code results. This result leads us to conclude that the GOA extensions to multi-trapping and thermal loading is validated.

4. HI retention in the upper plug of the ITER tokamak

The GOA and its extension are applied to estimate the tritium retention in a diagnostic upper port plug front surface, the diagnostics

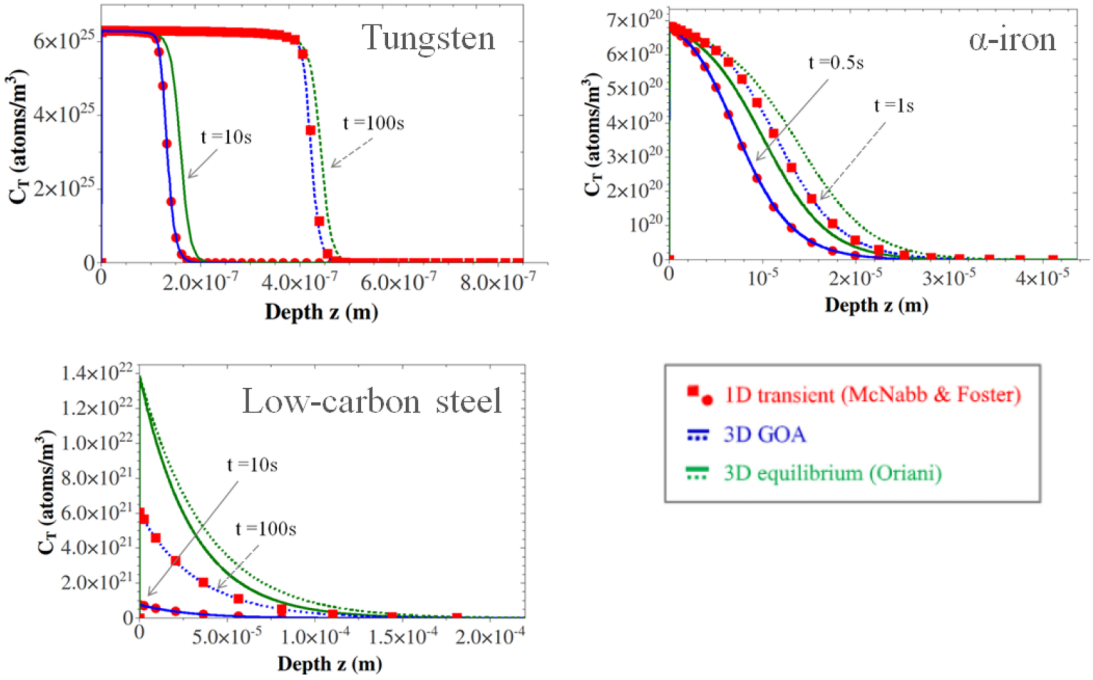

Fig. 1. Trapped hydrogen concentration along the beam for three different materials.

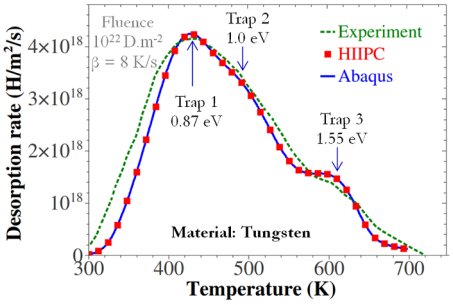

Fig. 2. TPD spectrum: experimental (green) from [17], simulation with the Generalized Oriani's formulation from Abaqus code (blue) and simulation with McNabb and Foster's formulation from HIIPC code (red). Simulations parameters are taken in [2]. (For interpretation of the references to colour in this figure legend, the reader is referred to the web version of this article.)

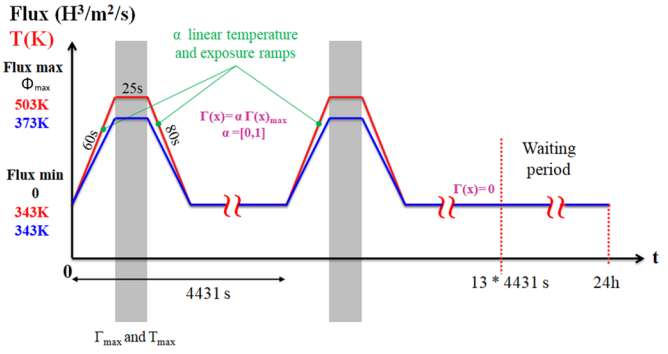

Fig. 3. One cycle (24 h) of the simulated scenario.

first wall (DFW) during deuterium-tritium operations of ITER tokamak. The DFW is made of 316 L stainless steel and is recessed behind the beryllium first wall to avoid direct plasma impact. The DFW is however exposed to energetic charge exchange neutral (CXN) particles. The plasma scenario considered here corresponds to a 25s-long $Q = 10$ D-T plasma, typical of the conditions expected at the beginning of fusion operations.

Fig. 3 illustrates the 24 h cycle scenario considered. 16 plasma pulses of duration of 25 s are assumed, according to the ITER Research Plan, over one day during those we assume a maximum HI implantation and an exposure surface temperature at 503 K and a cooling surface temperature of closer pipes at 373 K. During waiting periods, no HI are implanted and the temperature is considered at 343 K at both surfaces. Between exposure and waiting periods a HI implantation and surface temperature linear variations are assumed. Temperature fields in the sample are computed based on a steady state assumption. The geometry used for simulation is represented on Fig. 4a shows the considered geometry of the plasma-facing part and the applied boundary conditions, the temperature boundary conditions being time dependent. At the right the surface is exposed to the plasma; the bottom left represents a quarter surface of the cooling pipe. The temperature field showed in Fig. 4b corresponds to the steady-state temperature profile during plasma exposure.

In order to show the importance of thermal field and geometry on tritium retention, diffusion and transient trapping simulations on the 2D structure and on the equivalent 1D geometry (over the AB segment defined Fig. 4) are performed with Abaqus software (GOA).

Fig. 5 shows the temporal evolution of the total HI retention (solute and trapped) for 7 cycles obtained with 2D simulations and for an arbitrary plasma tritium flux of 4.1×10^9 H.m^{-2}.s^{-1}. The inventory increases rapidly during plasma pulses whereas desorption occurs between them. At the end of a week, the diffusion front (defined as the position from the exposure surface when tritium concentration is equal to 1% of the surface concentration) is around 0.3 mm. At this distance, 2D and 1D temperature fields are similar (see on Fig. 4b); consequently, the diffusion and trapping conditions are equivalent for these 7 cycles and there is no difference between the results obtained with a 1D and a 2D configuration.

Fig. 6 represents the relative difference on tritium retention between 1D and 2D configurations as a function of the diffusion front location. The difference ϵ is equal to:

$$\epsilon\,(\%) = \left| \frac{\iint_\Omega (C_T^{2D} + C_L^{2D})dxdy \; - L \int_A^B (C_T^{1D} + C_L^{1D})dx}{\iint_\Omega (C_T^{2D} + C_L^{2D})dxdy} \right| \times 100 \qquad (9)$$

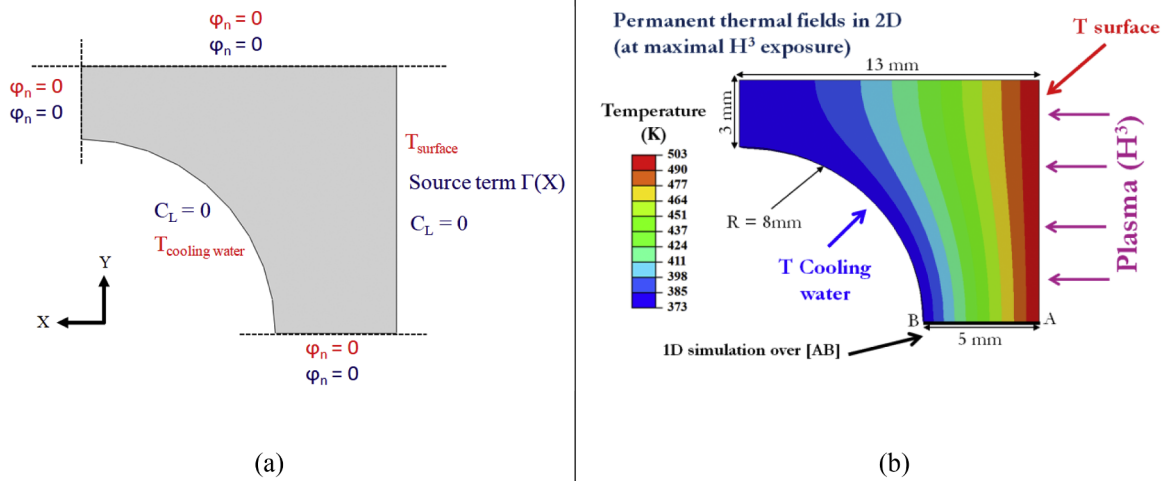

Fig. 4. (a). Symmetry and boundary conditions for temperature (red) and tritium concentration (blue). (b). Thermal field at the maximum tritium exposure. (For interpretation of the references to colour in this figure legend, the reader is referred to the web version of this article.)

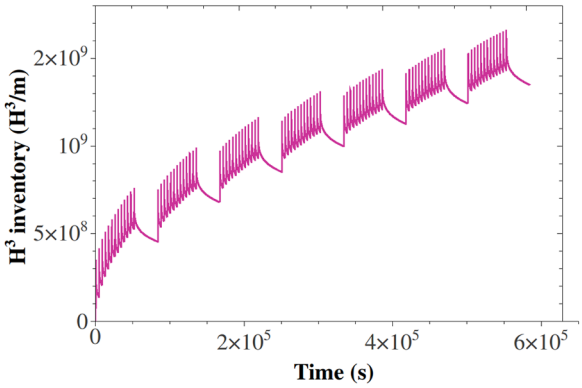

Fig. 5. Total tritium retention over the time (7 cycles of 24 h).

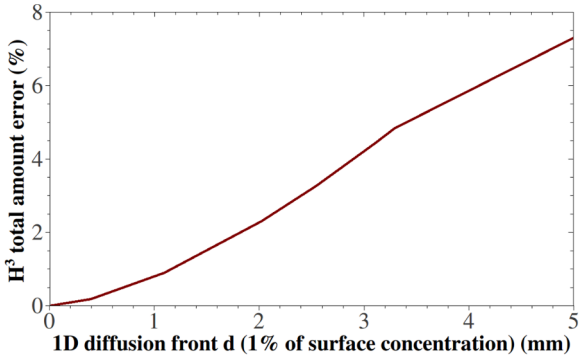

Fig. 6. Relative difference between 1D and 2D cases on total T retained over the diffusion front position (1% tritium concentration distance from the exposure surface).

where Ω is the 2D domain, L the y-length of exposure surface (11 mm). This figure was obtained by an application of constant high diffusive hydrogen concentration ($C_0 = 10^{20}$ H.m^{-3}), instead of the plasma source term, at the exposure surface, assuming that the discrepancies between the two case do not depend on the tritium implantation way. As previously discussed, when the diffusion front location is closed to the 'hot' surface, the relative difference is closed to 0, due to the very good correspondence between the 1D and 2D thermal fields. As the diffusion front goes deeper in the structure, the difference increase, up to 7% when tritium reaches the cooling pipe. Fig. 7 illustrates the solute (**7a**) and trapped (**7b**) 2D-map concentrations (normalized by C_0) in this last case. The concentration heterogeneities on the domain are due to the difference between thermal 2D and 1D equivalent thermal fields (which modified the diffusion and trapping behaviour) and geometries. Especially, an increase in the temperature leads to an increase of the detrapping process, and thus a decrease of the trapping concentration. Such special variation cannot be included directly in 1D computations: higher thermal gradient will increase the differences between 2D and 2D modelling.

5. Conclusion

A new transient HI trapping formulation based on the generalization of Oriani's formulation was proposed to ensure a correct convergence (and less computational cost) of commercial FEM codes. This Generalized Oriani's formulation was implemented in 3DS Abaqus code thanks to previous developments [8,9]. Direct confrontations with classical MRE approaches (based on McNabb and Foster's formulation) were done to valid the formulation and its implantation for a large set of diffusion/trapping material parameters. The TDS spectrum reproduction shows its capability to take into account multi-trapping and the thermal loading. At least, simulations were performed for 2D thermally active structure representative of a part of the diagnostic upper port plug front surface of the ITER tokamak. The difference on tritium inventory between 2D simulations and 1D equivalent case reaches 7% due to thermal field heterogeneities. For this case the discrepancy is low and it could be negligible in view of the general uncertainty of MRE simulations. Furthermore, considering the numerical costs needed to multidimensional calculations, 1D simulations remain relevant approach to estimate, as a first approximation, the HI inventory. However, for more general or complex configurations, 2D or 3D simulations are useful to ensure the validity of 1D simulations, and/or to improve them, especially in term of equivalent parameters used. Last, it is worth noting those thermal field heterogeneities, beside inducing differences between 1D and 2D computations, should induce heterogeneous mechanical fields (due to the thermal expansion), which might affect, in return, the HI transport in sample through the induced hydrostatic pressure.

Acknowledgments

This work has been carried out within the framework of the EUROfusion Consortium and has received funding from the Euratom

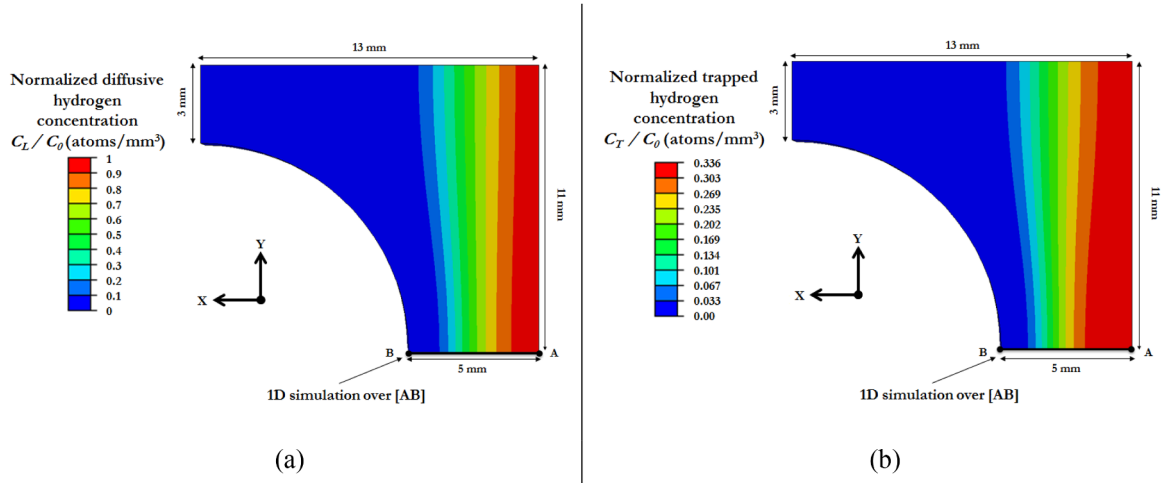

Fig. 7. (a). 2D-map of solute hydrogen concentration (normalized by C_0). (b). 2D-map of trapped hydrogen concentration (normalized by C_0).

Research and Training Program under grant agreement CFP-WP14-WPPFC. The views and opinions expressed herein do not necessarily reflect those of the ITER Organization or the European Commission. ITER is a Nuclear Facility INB-174. This work is also part of the WHISCI and WHeSCI projects http://piim.univ-amu.fr/amidex/whesci, that have received funding from the Excellence Initiative of Aix-Marseille University - A*MIDEX, a French “Investissements d'Avenir” programme.

References

[1] G.R. Longhurst, J. Ambrosek, Fusion Sci. Technol. 48 (2005) 468–471.
[2] E.A. Hodille, X. Bonnin, R. Bisson, T. Angot, C.S. Becquart, J.M. Layet, C. Grisolia, J. Nucl. Mater. 467 (2015) 424–431.
[3] C. Sang, X. Bonnin, M. Warrier, A. Rai, R. Schneider, J. Sun, D. Wang, Nucl. Fusion 52 (2012) 043003.
[4] O.V. Ogorodnikova, M.A. Fütterer, E. Serra, G. Benamati, J.F. Salavy, G. Aiello, J. Nucl. Mater. 273 (1999) 66–78.
[5] A. McNabb, P.K. Foster, Trans. Metall. Soc. AIME 227 (1963) 618–627.
[6] C. Quirós, J. Mougenot, G. Lombardi, M. Redolfi, O. Brinza, Y. Charles, A. Michau, K. Hassouni, Nucl. Mat. Ener. 12 (2017) 1178–1183.
[7] A.H.M. Krom, R.W.J. Koers, A.D. Bakker, J. Mech. Phys. Solids 47 (1999) 971–992.
[8] Y. Charles, T.H. Nguyen, M. Gaspérini, Int. J. Mech. Sci. 120 (2017) 214–224.
[9] Y. Charles, T.H. Nguyen, M. Gaspérini, Int. J. Hydrog. Energy 42 (2017) 20336–20350.
[10] Y. Charles, M. Gaspérini, K. Ardon, S. Ayadi, S. Benannoune, J. Mougenot, Procedia Struct. Integrity 13 (2018) 896–901.
[11] R.A. Oriani, Acta Metall. 18 (1970) 147–157.
[12] S. Benannoune, Y. Charles, J. Mougenot, M. Gaspérini, Int. J. Hydrog. Energy 43 (2018) 9083–9093.
[13] S. Benannoune, Y. Charles, J. Mougenot, M. Gaspérini, “Generalized Oriani's Approximation domain of validity”. To Be Published.
[14] P. Sofronis, R.M. McMeeking, J. Mech. Phys. Solids 37 (1989) 317–350.
[15] K. Radhakrishnan, A.C. Hindmarsh, Description and use of LSODE, the Livermore Solver for Ordinary Differential Equations, Lawrence Livermore National Laboratory (1993).
[16] Simulia, Abaqus User Subroutines Reference Guide, Dassault Système (2011).
[17] O.V. Ogorodnikova, J. Roth, M. Mayer, J. Nucl. Mater. 313-316 (2003) 469–477.